Int J Adv Manuf Technol (2014) 74:481–502
DOI 10.1007/s00170-014-5959-4

ORIGINAL ARTICLE

Real-time fuzzy-clustering and CART rules classification of the characteristics of emitted acoustic emission during horizontal single-grit scratch tests

James Griffin · Xun Chen

Received: 28 January 2014 / Accepted: 13 May 2014 / Published online: 6 June 2014

Abstract During the unit event of material iteraction in grinding three phenomena are involved, namely: rubbing, ploughing and cutting. Where ploughing and rubbing essentially mean the energy is being applied less efficiently in terms of material removal. Such phenomena usually occurs before or after cutting. Based on this distinction, it is important to identify the effects of these different phenomena experienced during grinding. Acoustic emission (AE) of the material grit interaction is considered the most sensitive monitoring process to investigate such miniscule material change. For this reason, two AE sensors were used to pick up energy information (one verifying the other) correlated to material measurements of the horizontal scratch groove profiles. Such material measurements would display both the material plastic deformation and material removal mechanisms. Accurate material surface profile measurements of the cut groove were made using the Fogale Photomap Profiler which enables the comparison between the corresponding AE signal scratch data. By using short-time Fourier transforms (STFT) and filtration, the salient features for identifying and classifying the phenomena were more distinct between the three different levels of single-grit (SG) phenomena. Given such close data segregation between the phenomenon data sets, fuzzy clustering/genetic algorithm (GA) classification techniques were used to classify and verify the demarcation of SG phenomena. After the cutting, ploughing and rubbing gave a high confidence in terms of classification accuracy, the results from the unit/micro-event to the multi/macro-event, both 1-μm and 0.1-mm grinding test data, were applied to the named classifier for classification. Interesting output results correlated for the classifier signifying a distinction that there is more cutting utilisation than both ploughing and rubbing as the interaction between grit and workpiece become more involved (measured depth of cut increases). With the said classifier technique it is possible to get a percentage utilisation of the grit and material interaction phenomena. In addition, optimised fuzzy clustering was verified against a classification and regression tree (CART) rule-based system giving transparent rule classification. Such findings were then realised into a Simulink model as a potential control system for a micro-grinding simulation or, for real-time industrial control purposes.

Keywords Single-grit scratch · Acoustic emission · Feature extraction · Fuzzy clustering · Genetic algorithms · CART rules · Simulink simulation

Nomenclature

AE	Acoustic emission
C	Cutting
CART	Classification and regression tree
DOC	Depth of cut
DSP	Digital signal processing
FFT	Fast Fourier transform
Hit 17	Scratch number 17
P	Ploughing
R	Rubbing
RMS	Root mean squared
STFT	Short-time Fourier transform
SG4/SG	Single-grit trial 4/single grit
T210/T212	Test 210/test 212
WPT	Wavelet packet transforms

J. Griffin (✉)
University of Chile, Pizo 4, Torre Central, Beauchef 850, Santiago, Chile
e-mail: jgriffin@ing.uchile.cl

X. Chen
Liverpool John Moores University, Room 5, GERI Building, Byrom Street, Liverpool L3 3AF, UK
e-mail: X.Chen@ljmu.ac.uk

1 Introduction

Material particle displacements can be observed from the emitted elastic waves that propagate through material media [1, 2] when an object is subjected to an external force in terms of an initiated material stress. The released energy is primarily in the form of an acoustic emission (AE). From various stresses, there are material particle displacements, which are associated with AE and released in the form of material elastic energy. These elastic AE waves mimic the mechanical vibration of material and grit interaction and are extracted by AE sensors. Different AE characteristic signals are analogous to different external forces that act on the same material or the same force exerted on different materials [3, 4]. Elastic waves can therefore be used for monitoring many machining processes and/or material non-destructive tests [5–9].

AE monitoring may be a difficult task; however, with correct data, it is possible to monitor grinding phenomena features of interest. For example, such phenomena could be the level of burn or machine chatter marks or, more importantly, the efficiency of the grinding cut. The latter is of particular importance to this research in that single-grit (SG) scratch experiments are important to the understanding of the micro-aspects endured during the grinding of workpiece materials. Previous research by Griffin and Chen and Chen et al. [3, 4] looked at CMSX4 (heat-resistive aerospace materials, see Table 1) and other aerospace alloys with rotating radial scratch indented on two equally spaced workpieces (180° apart). With horizontal scratches, the comparison between grinding wheel and SG scratch are more accurate, as it is easier to control the depth of cut (DOC) on a flat plain whereas this is not the case with the rotating scratch tests. In this paper, there is a focus on identifying the different levels of cutting phenomenon in grinding. It can be said that varying levels of SG interaction is an easier phenomenon to observe when compared with that of grinding. This is in terms of the distinguishing features between cutting, ploughing and rubbing and the irregular distribution of grains when interacting with the material workpiece. Once the observations and associated data has been achieved to distinguish between different features, it can then be used to look at different levels of cutting, ploughing and rubbing experienced in grinding. There has been a lot of work on SG analysis previous to this work where the material removal mechanisms were investigated from microscopic analysis and acquired force signals [10–12].

The AE wave is described as a non-stationary stochastic signal. AE extraction has been used in many machining processes from milling, drilling to grinding where AE signals extracted from the material tests would traditionally use root-mean-squared (RMS) level detection, event count, energy distributions, amplitude and the powers of dominate frequency bands [4]. These techniques were broadly used and applied to general non-destructive condition monitoring tests based on events that were recorded in days instead of seconds. With SG scratch tests, the different grinding phenomena are produced by both short-high- and long-low-frequency components. To that end, there is a need to use continuous recorded AE data and capture all the information present. The raw AE peak-to-peak data is used for SG tests as RMS AE data can again miss out important information where high-frequency information is usually contained within the raw-extracted AE data. To date, little work has looked at the energy relationships experienced during SG scratch tests in grinding. However, this has been looked at in other areas of research such as the characteristics of AE during single diamond scratching of granite [13], where the RMS AE is extracted for different materials and different processes of rock cutting where the major mechanisms are microchipping, crack propagation and sliding friction, which are similar to cutting, ploughing and rubbing.

For all the scratch tests carried out in this paper, the AE waveforms were normalised to 1-μm cut (significant to cutting DOC) depths to compare like with like signals (where signals were compared on frequency feature matching and not just DOC). SG scratching segregating different physical phenomenon through AE waveforms is a novel approach especially when applied to aerospace materials. Signal normalisation is required for application into expert rules with non-conflicting cases (normalisation mainly applies to just cutting and ploughing, as these were the most difficult phenomena to segregate, rubbing however was mainly extracted during the previous pass to the actual scratch with marked plastic deformation).

Other relevant research investigates AE related to the proposed research within this paper. One that is particularly interesting is the application of wavelet transforms with a fuzzy neural network used to determine the wear states from correlated AE during drilling 40Cr steel [14]. By using fuzzy neural networks, it is possible to quantify overlapping wear states through AE signals, which is fundamental to the work here. More recently, investigations look further at wear mechanisms experienced in micro-milling which again quantifies how AE can be used to distinguish such microscopic phenomena [15]. Ren et al. also looks into other precision machining where fuzzy identification using extended subtractive cluster analysis and least squares gives an adaptive filter capability that when tuned can accurately measure material removal mechanisms, giving the process more accuracy against unwanted noise [16]. The research discussed in this paper utilises such ideas in indentifying more microscopic features achieved during event-driven AE signals of SG grinding scratch tests. Moreover, the precision of AE technologies applied to wear can be directly related to material removal mechanisms achieved during SG scratch tests.

The main investigation objectives of this paper are:

- Characterise cutting, ploughing and rubbing phenomena in horizontal SG scratch tests using material

profile measurement techniques correlated to AE signal events.
- Analyse cutting, ploughing and rubbing of both normalised and non-normalised signals for SG interaction of CMSX4 aerospace material (see Table 1).
- Compare cutting, ploughing and rubbing with non-normalised signal for SG interaction of Titanium 64 (see Table 1)
- Classify cutting, ploughing and rubbing in grinding with 1-μm and 0.1-mm cutting depths.
- Classification using fuzzy clustering with GA optimisation classifying the level of percentage utilisation for cutting, ploughing and rubbing.
- Verified classification using the CART transparent rules signifying the frequency bands of interest.
- Produce a cutting, ploughing and rubbing simulation with the perspective of real-time application.

The investigations of SG horizontal scratch work in extracting AE waveforms to identify the energy footprints of cutting, ploughing and rubbing during conventional grinding is both novel or provides a different focus in obtaining efficient cutting conditions especially when applied to a simulation for real-time realisation or higher fidelity models. The rest of the paper is organised into the following sections: Sect. 2, signal processing for AE; Sect. 3, experimental setup; Sect 4, AE and SG tests; Sect. 5, optimised fuzzy-clustering classifier; Sect. 6, optimised fuzzy clustering classification results for cutting, ploughing and rubbing; Sect. 7, CART classification results for cutting, ploughing and rubbing; Sect. 8, SG simulation; and Sect. 9, conclusions.

2 Signal processing for acoustic emission

Using just the raw extracted time signal only gives the user one perspective of the AE properties. With fast Fourier transforms (FFT) however, it is possible to get the frequency band components. The FFT estimates the frequency components as well as their associated amplitudes based on the trigonometric family functions. FFTs have been used for condition monitoring in the past albeit they do not give any time information of when the event occurred [9].

With this weakness in mind, there is a need for FFT to be represented in the time domain and this paved the way for short-time Fourier transforms (STFT). A similar function to FFT albeit the FFT is calculated over equally spaced time slots correlated against the raw extracted time signal. There is a trade-off between frequency and time resolution, which is needed for accurately distinguishing SG features in a noisy environment. That said, and with the extra-dimension of time, the STFT still offers a good solution when required to characterise an AE signal for SG scratches amongst other grinding phenomena.

Where Eq. 1 introduces the STFT [17]:

$$\mathrm{STFT}_{x}^{(\omega)}(t',f) = \int_{-\infty}^{\infty} [x(t) \times w*(t-t')] \times e^{-j\pi ft} dt \qquad (1)$$

as with Eq. (1), $x(t)$ is the time domain signal under transform, $w(t)$ is the main difference from FFT and is known as the window function and * is the complex conjugate. Based on the increment value of t', this will determine the resolution between the frequency and time domains.

The present investigation is motivated by the expectation that AE features of SG cuts can be extracted clearly by using STFT. Investigation and classification of such waveforms provides a profound initial step in understanding and distinguishing the very fundamentals of grinding interaction, which can ultimately increase the effectiveness of grinding monitoring. Once the raw extracted AE has been transformed into the time-frequency domain, it can then be presented to the classifier. Here, the work looks at the SG scratch classification of cutting, rubbing and ploughing using the classifier: fuzzy clustering with genetic algorithm (GA) optimisation. Moreover, it was found that the STFT results of AE analysis can represent different characteristics of cutting, ploughing and rubbing in grinding, which may be used as input parameters for the classification. The classification of the three phenomena is of particular importance to the fundamental understanding of grinding mechanics. Not just classifications are given, percentage utilisation and the transparency of generalistic verified rules relating to frequency bands of interest are also given.

Table 1 Displays aerospace material properties used in this work [22]

Property	CMSX4	Titanium-64
Composition (wt.%)	Mo, 0.6; Cr, 7; Ti, 1; Al, 5.6; Co, 10; Ni, 67; Re, 3; and W, 6	C, 0.08; Al, 5.5–6.75; Fe, 0.30; and H, 0.010
Density (kg/m^3)	8,690	4,650
Hardness	520 HV	349 HV
Tensile strength (MPa)	1,090	950
Yield strength (Mpa=N/mm^2)	990	880
Elastic modulus (GPa)	18.5	109.6
Elongation (%)	10–12	14
Melting point (°C)	1,395	847
Passion's ratio	0.273	0.34
Thermal conductivity (W/mk)	12~63	6.70
Special heat capacity (K/kgK)	381~544	450
Thermal diffusivity (×10^{-6} m^2/s)	2.54~21	16

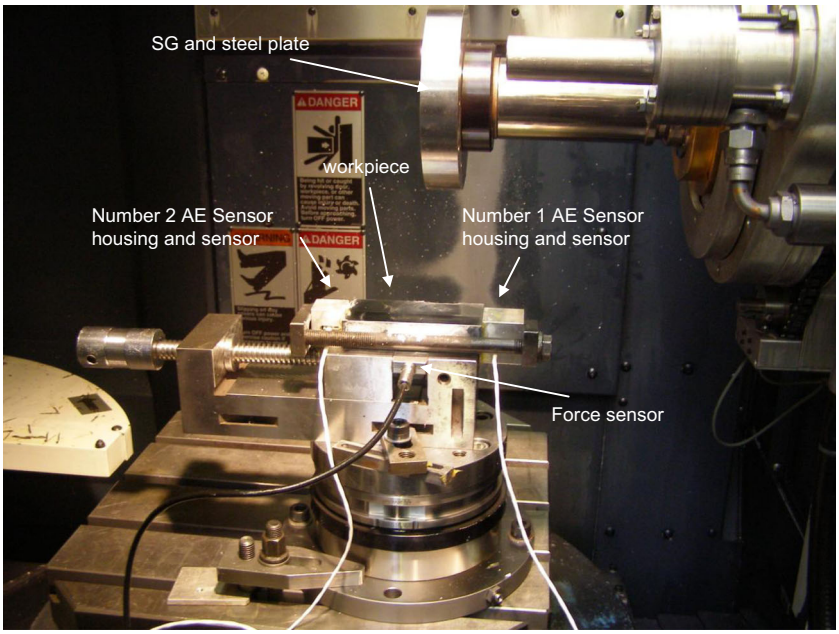

Fig. 1 Makino A55 grinding centre machine setup for horizontal SG scratch test

3 Experimental setup of horizontal SG scratch tests

The AE associated with grinding chip formation may be investigated by a scratch simulation of grinding. The experiment of SG scratch test was carried out on a specially designed rig fixed within a Makino A55 Machine Centre as shown in Fig. 1. The aerospace alloys CMSX 4 and Titanium 64 were chosen for the SG tests and all samples used were polished to a very high quality (R_a=0.01 μm), which give the tests further confidence with respect to measurements. Such materials were chosen to give different material characteristics when exerted with a source of initiated stress.

A SG was glued into a microscopic drilled hole of the specially designed steel plate. The steel plate would then be fixed to the spindle and rotated at commercial grinding speeds. The SG was fixed to the plate in a protruding fashion which would ensure the SG was the 1st object to make contact with the workpiece when controlled within a micron of accuracy.

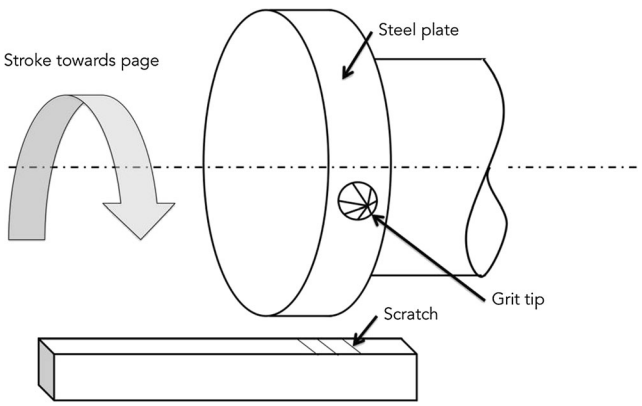

Fig. 2 Sketch of horizontal SG scratch test rig

The scratch test was carried out by feeding a rotating Al_2O_3 grit towards a flat horizontally placed workpiece as illustrated in Fig. 2. With a micron incremental grit stroke, a scratch groove can be formed on the surface of the flat sample. The average scratch depth is about 1 μm, which is a typical value of grinding chip in high efficiency grinding. The scratching wheel rotational speed is 4,000 RPM with a feedrate of 4,000 mm/min under down-grinding condition.

During a single scratch action, the AE feature frequency bands/intensities change with respect to time. In short, the mechanical AE propagation should be considered in both time and frequency features where the prominent AE feature frequencies of the scratches are in the range 100~550 kHz, which are similar to the AE feature frequencies in grinding tests experienced in previous work [4].

An AE data acquisition system where two physical acoustics WD AE sensors were used both identical and with a frequency response range at 80 kHz to 1 MHz. The two sensors were set up equal distances apart (see Fig. 1 for setup configuration). The sampling rate was set to 5 MHz to ensure no aliasing occurred when the signal was filtered and reconstructed using the Matlab DSP Toolbox, and all the short burst high-frequency information was obtained.

4 Acoustic emission in SG scratch tests

When the process of grit to workpiece interaction occurs, the AE is emitted as a material stress-release process. This emitted AE during the scratch may come from elastic or plastic shear stress due to material removal or material deformation mechanisms. The process of identification between various mechanics of grinding (cutting, ploughing and rubbing) can be

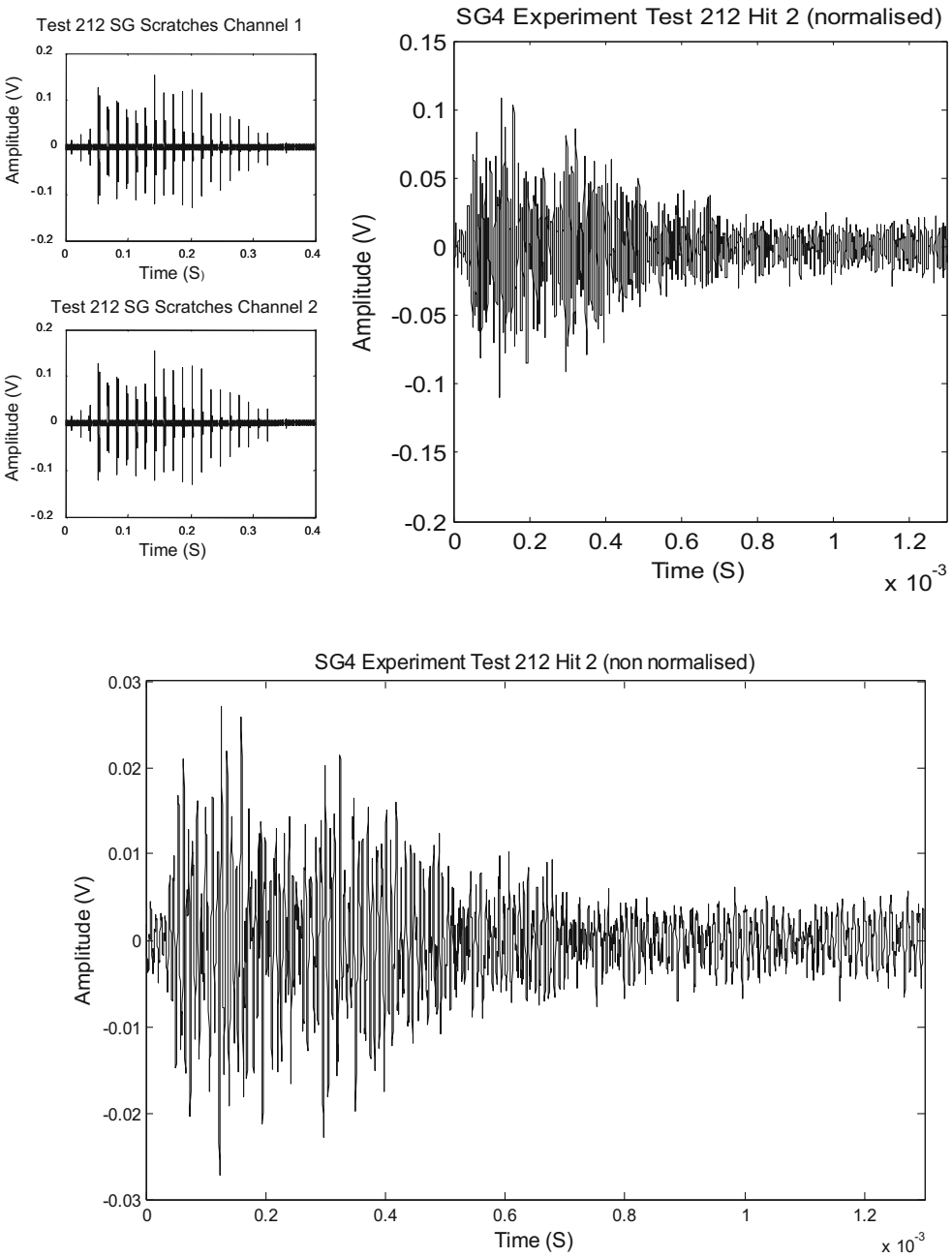

Fig. 3 Machine, Makino A55; SG material, Al_2O_3; workpiece, CMSX4; SG dimensional depth and width approximation, 1 μm; dry down grinding, V_s= 4,000 RPM; V_w=4,000 mm/min; A_p=0.001 mm. *Top left*, two channels for test 212 hit 2 (normalised), *top right*, raw extracted time signal; and *bottom*, test 212 hit (raw extracted signal)

found in Refs. [3, 18]. Figure 3 shows the AE signals of a SG scratch test (T212) from two PAC WB AE sensors. Both hit 2 normalised (top right) and hit 2 non-normalised (bottom) are displayed. With reference to the phenomena displayed from the STFT representations of AE T212 hit 2 in Fig. 4 (top); the measured cut length was 401 μm. T212 refers to test 212 where many sequential scratches were found as the grit interacted more with the workpiece. Hit 2 refers to the second profile grit scratch groove where the length tends to increase due to more interaction between both grit and workpice. T210 and T211 are reference to the tests carried out previously (every test the grit increments 1 μm closer to the workpiece material) where AE from slight elastic touching thus signifying the onset of rubbing phenomenon.

Looking at both top and bottom of Fig. 4, it is possible to see that the normalised STFT of Hit 2 is similar to the normalised signal of hit 17 where hit 17 required less normalisation as DOC was recorded near 1 μm. Looking between the two STFTs, there is more information in terms of frequency bands for hit 17; however, the general patterns for the material removal mechanisms are essentially the same and with such normalisation can be used in a generalised AE control system/high fidelity model.

From actual DOC and SG analysis without normalisation, there is a relationships from the DOC and registered

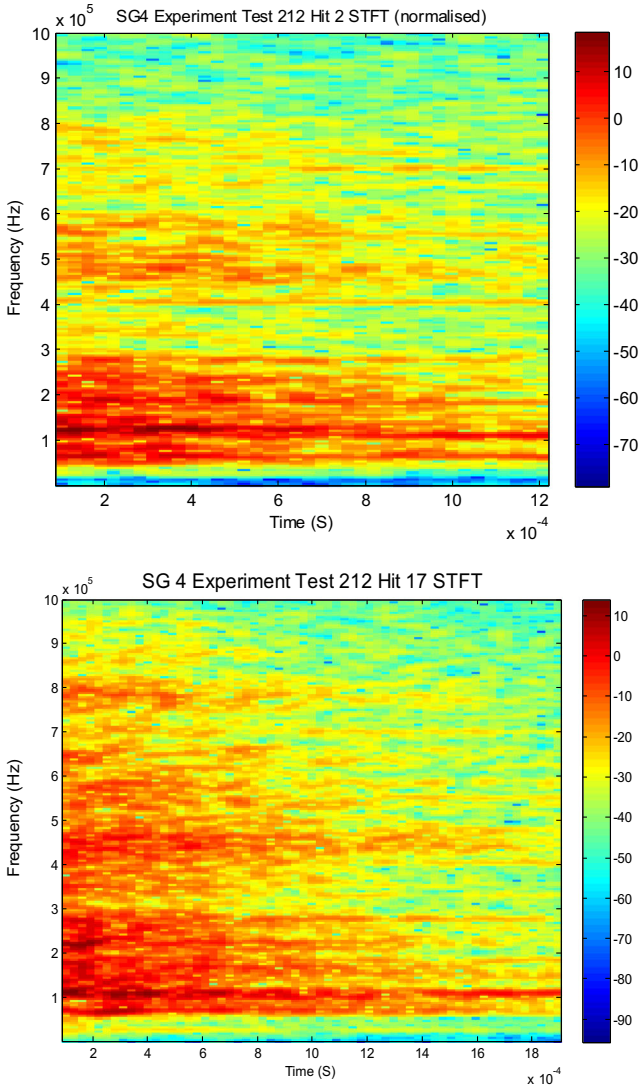

Fig. 4 *Top*, SG4 test 212 hit 2 displays the normalised STFT; *bottom*, SG4 test 212 hit 17 displays the normalised STFT

amplitude; however, for different materials, there are different dominate frequency bands; this is due to signals being able to oscillate more freely in less damped material due to lower levels of hardness and more dense materials for example (see Table 1). For introduction to the classifier, there is a need to only supply the normalised data as non-normalised data gives problems with overlapping contradictory data. That said, such classifiers can strip off absolute measurements where the non-normalised is used for various material interactions (absolute measurements sent to another part of the classifier where the DOC is distinguished separately) and normalised measurements are used to compare like against like in terms of the emitted material stress signatures.

Pencil break tests [19, 20] also displayed a large response time to what can only be described as a microsecond fracture; Griffin et al. [3] display this calibration phenomenon with a synchronised downward force signal (Fz). In this work, it can be seen that the AE-extracted pencil fracture is represented by a recorded 50 N force; however, the 50-N force is captured over a much longer time period, which is representative of the applied force and not the actual fracture [3]. This method of AE sensor calibration has been used in grinding technologies before [21]. Important points to take here is we can calibrate the AE energy to force and on a daily basis get a normalised level amount for trial comparisons taken at different times/environmental conditions. Figure 4 top displays the full normalised STFT for hit 2 and below the full normalised STFT for hit 17, all taken from scratch Test 212 (Fig. 5). Figure 5 shows the 3D scratch profile created by SG4 Test 212 Hit 17.

Figure 6 (top) represents the FFT slices obtained from the STFT (reference to Fig. 4, bottom) relating to the horizontal cross-sectional cut profiles (taken from Fig. 5), which signify whether the signal is cutting, ploughing or rubbing based on the material equation [3]. All phenomena occupy the same peak frequency bands; however, the higher amplitudes are for cutting, then next, ploughing and lastly, in between the machine noise with a magnitude between 0.3 and 0.8 is the rubbing phenomenon.

From those patterns, ploughing occupied between 80 and 300 kHz of the major frequency band peaks with normalised magnitudes between 1 and 2 and sidebands between 0.7 and 1.4. Cutting also had similar major frequency band peaks between 80 and 300 kHz. The normalised magnitude for the major band peak was between 2.4 and 4 with side bands the same or slightly less than that of the ploughing side band magnitudes. Both ploughing and cutting have slight frequency band peaks around the 500-kHz range, and cutting has slightly larger peaks when compared with rubbing and ploughing at the 750-kHz range. Rubbing has major frequency bands between 80 and 500 kHz with the major peaks ranging from 0.3 to 0.8 magnitudes.

With the different energy signatures occurring from the SG interacting within the workpiece, STFT provides a good solution for separating the cutting, ploughing and rubbing phenomena. Ploughing and cutting are somewhat similar in that the material is push/slided to one side or material removed, respectively, as these predominately cause material plastic deformation. The energy is consumed from surface deformation. From taking the major frequency band intensities, this is significant to the first harmonic, which is significant to 97 % of the emitted AE energy. In the rubbing case, however, there is surface friction [22], which suggests therefore, that different AE signatures should be apparent between the two different phenomena. Rubbing does not remove or slide any material away, instead, it touches the surface with no visible markings, which signifies elastic material characteristics in that the material deforms and returns back to its original state after a SG pass has occurred. In short, the boundaries are much closer in terms of AE distinguishing features of ploughing and cutting.

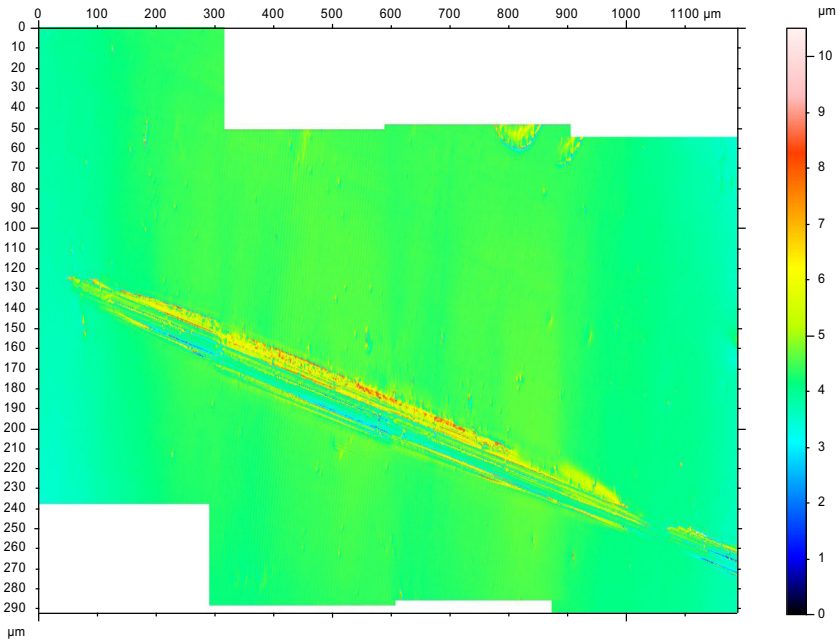

Fig. 5 SG4 test 212 Hit 17 3D mountains scratch profile

Ploughing and cutting are perhaps the most difficult phenomenon to separate based on this assumption which further signifies the need for an accurate classifying technique. Not just an accurate technique but also a technique that provides the grinding phenomena in terms of percentage utilisation. In addition, another desirable feature of a classifier is to provide meaningful transparent rules to directly relate to frequency bands of interest.

The first part of the section looks at the SG tests for use in classifier technologies, which requires normalisation; however, a discussion is required in terms of its mechanical and electrical outputs. The next part of this section discusses two

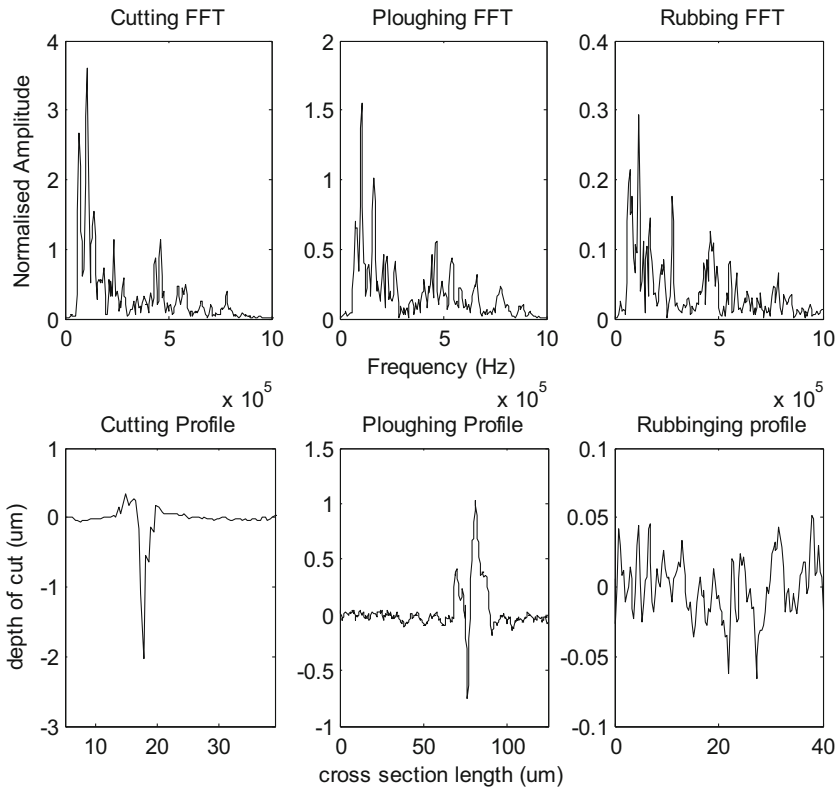

Fig. 6 FFT slices (*top*) and profiles relating to cutting, ploughing and rubbing phenomenon for CMSX4 material (*bottom*)

SG tests in terms of non-normalised signals and that of the actual SG phenomenon's, namely cutting, ploughing and rubbing. For the non-normalised tests, two different aerospace materials are used to provide discussion in terms of comparisons when generalising SG models (see Table 1 for information of the two investigated materials).

Figure 7 displays the non-normalised STFT of the rubbing phenomenon, which was obtained as the first hit or AE pickup for Test 210, where no mark was present on the CMSX4 workpiece surface, which is indicative of rubbing.

Figure 8 displays the non-normalised AE STFT which allows the distinction of cutting and ploughing when higher material removal mechanisms are measured tending towards a max of 1.5 μm. The higher material removal indicative of cutting is based at the beginning of AE just after the initial rubbing and ploughing tending towards the max DOC (negative apex of the grit and material). After this phenomenon as the amplitudes and the DOC decreases this is then significant of the ploughing phenomenon.

Looking at Fig. 12 (top for CMSX4), the power spectrum density (PSD) can be seen for all phenomena where PSD is at its greatest for cutting, then ploughing and significantly less for rubbing. Such signal analysis can be used for distinguishing general features such as DOC and general energy bands of different materials.

From recent work investigated by Opoz [23], such SG results investigate a more focused view in terms of the mechanics behind cutting, ploughing and rubbing. Such findings made in Opoz and Chen's work [23] further reinforce the findings made here. For example, Opoz et al. [23] talks about material moving starting just after the initial touch and the first initial low depths of cut, which is significant to initial ploughing. The work carried out in this paper uses the material removal mechanisms given by Griffin and Chen [3] for

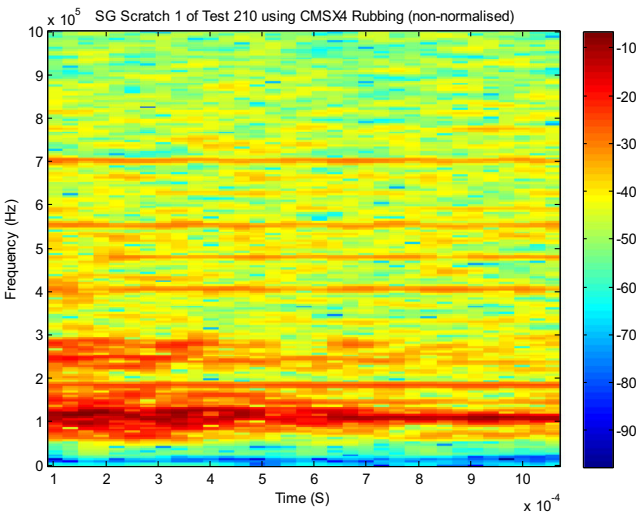

Fig. 7 SG4 test 212 hit 210 displays non-normalised STFT of the rubbing phenomenon

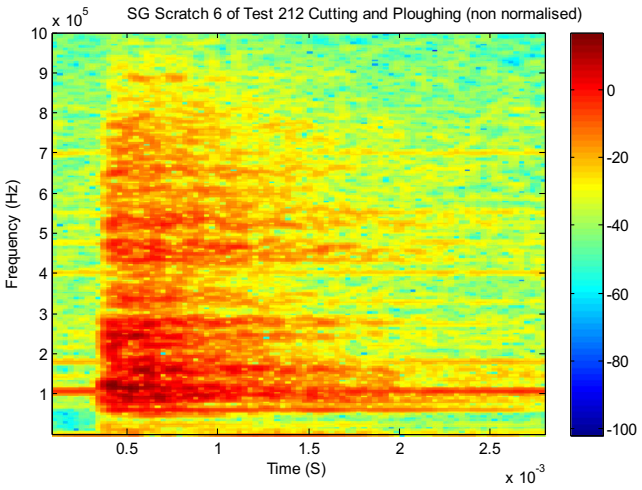

Fig. 8 SG4 test 212 hit 6 displays the non-normalised STFT of both cutting and ploughing phenomena

determining cutting, ploughing and rubbing, and such cutting-correlated signals were only found in the initial part of the scratch tending towards the maximum DOC (from low initial DOC to the centre of the scratch). Looking at the non-normalised STFT of Scratch number 6 it can be seen the initial levels of ploughing from low DOC are then immediately replaced with cutting phenomena where higher AE intensities are experienced as the grit with material approaches maximum DOC. The signal intensities either side of this phenomenon were indicative of ploughing which again correlates with the work carried out by Opoz et al. [23]. Looking again at Fig. 8 just after cutting, there are large amounts of the ploughing phenomenon, which is consistent with the findings made by Opoz et al. [23]. This paper and previous related work focuses more on energies emitted in the form of AE events where Opoz et al. focuses more on material removal mechanisms where both bolsters work in SG modelling to the grinding community at large. Finally, the rubbing phenomenon which was found from AE signal pickup correlated to a none-representative mark, was assumed to be elastic in nature. Such rubbing phenomenon was found in the previous test; Test 210 where no marks were recorded on the workpiece and intensities consistent with AE scratch number 1 (Fig. 3, top left) where again such AE signal event was recorded although with no physical mark located on the surface (It was on the next test when scratches were formed along the surface, T212). The work in this paper concentrates on similar investigations made by Opoz et al. [23]; however, with the addition of an AE sensor, it was possible to see such miniscule grit and material interactions with a view of changing intensities that supports such technology when used in a real-time manner (see Sect. 8 for example system).

The following part of this section discusses signals obtained from SG trial number 5 using the aerospace material,

Titanium 64. In contrast with the last part of the SG trial number 4, the signals in this part are non-normalised and so the intensities can be compared with the last part of SG4 using CMSX4 material where different materials emit different frequencies when interacted with a rotating SG Al_2O_3 material. Only the normalised levels of the material CMSX4 were used for classification and simulation results. That said, equally the Titanium 64 AE signals can be easily normalised and used alongside CMSX4 data due to the different frequency bands for the different phenomena.

Figure 9 is somewhat different to Fig. 6 as this figure relates to a non-normalised AE event and Fig. 6 AE event is normalised to 1 μm, which signifies the difference between the dominant amplitudes, which is correlated with DOC. Titanium 64 is discussed in terms of different material removal mechanisms correlated to the measured AE event.

In comparing the non-normalised signals of Figs. 7 and 8, it can be seen that the rubbing phenomenon of Titanium 64 is similar to that seen with CMSX4, with reference to Fig. 3 and previous results investigated by Griffin et al. [3]. This is certainly true in terms of intensities; however, the emitted spectrum of the recorded AE-emitted signal have much higher frequency components when compared with that of CMSX 4; this can be attributed to two factors: Titanium 64 is a much more combustible material, and with less hardness/material density than CMSX4, the emitted AE can vibrate more with less material damping. Such assumptions are further amplified when looking at Figs. 10 and 11, where greater intensities are found due to cutting and ploughing material removal mechanisms recording slightly higher DOC (same setup for both material trials using a A55 machine centre with 1 μm increments). The intensities however correlate with the CMSX4 non-normalised AE of Fig. 8. For example, when comparing the sliced STFT with material phenomena of Fig. 9 with that of Fig. 6, Fig. 9 is non-normalised to 1.5 μm DOC where Fig. 6 is normalised to 1 μm.

Therefore, it is expected that Fig. 9 has higher intensities due to the measured higher DOC, however when comparing Fig. 8 with Fig. 11, the two non-normalised STFT give similar intensities. The time series signal of Fig. 11 (top) is similar in amplitude to that of the normalised signal of Fig. 3 (top right). With similar setups, the time signals give good correlation to similar emitted AE signals for both materials.

Such considerations need to be taken into consideration when realising a general model for SG. With such findings, it is necessary to have focused material SG models that are normalised to give accurate output. From the normalised AE SG signals, the different intensities can be handled with the addition of another expert classifier giving correlation to DOC.

With dedicated normalised classifiers, it is possible to use SG tests as an intelligent material footprint to calibrate the control of automated grinding machine centres. To amplify the robustness levels in segregating two materials in terms of cutting, ploughing and rubbing (Fig. 12), PSD energy curves are similar for both materials; however, a change in sharpness is recorded between Titanium 64 and CMSX 4. Such patterns can be used in addition with STFT and time series to give more accurate classifications.

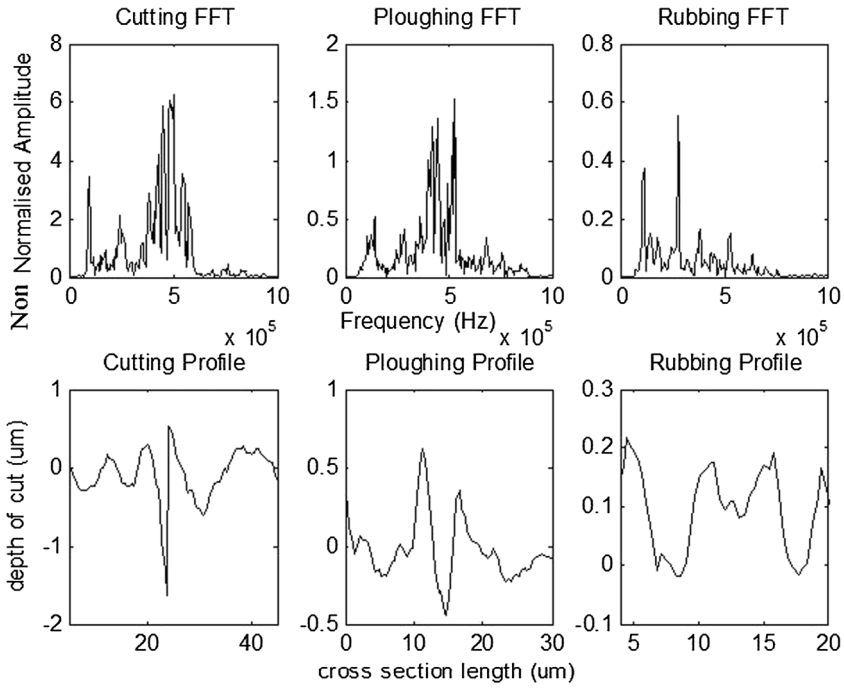

Fig. 9 FFT slices (*top*) and profiles relating to cutting, ploughing and rubbing phenomenon for titanium 64 material (*bottom*)

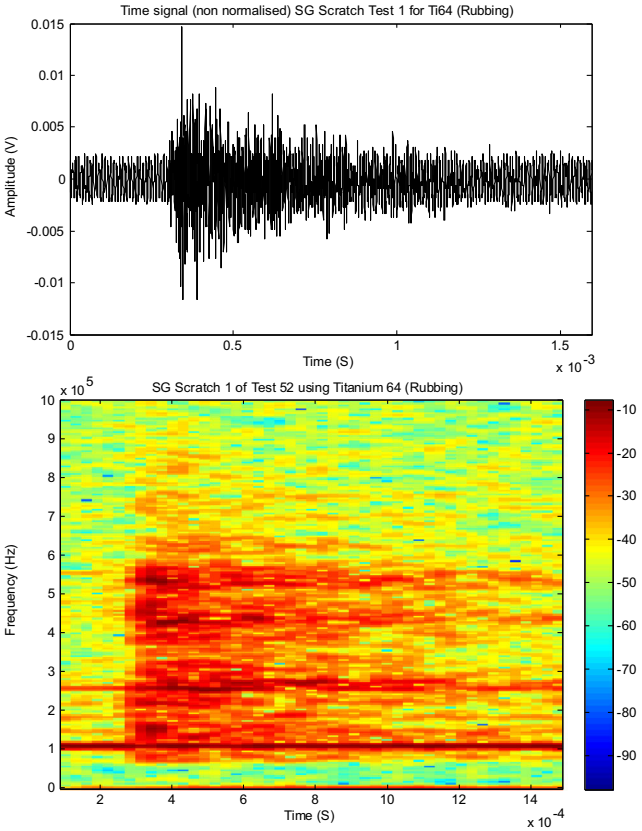

Fig. 10 *Top*, AE time series signal of rubbing phenomenon for titanium 64 material; *bottom*, STFT of TOP

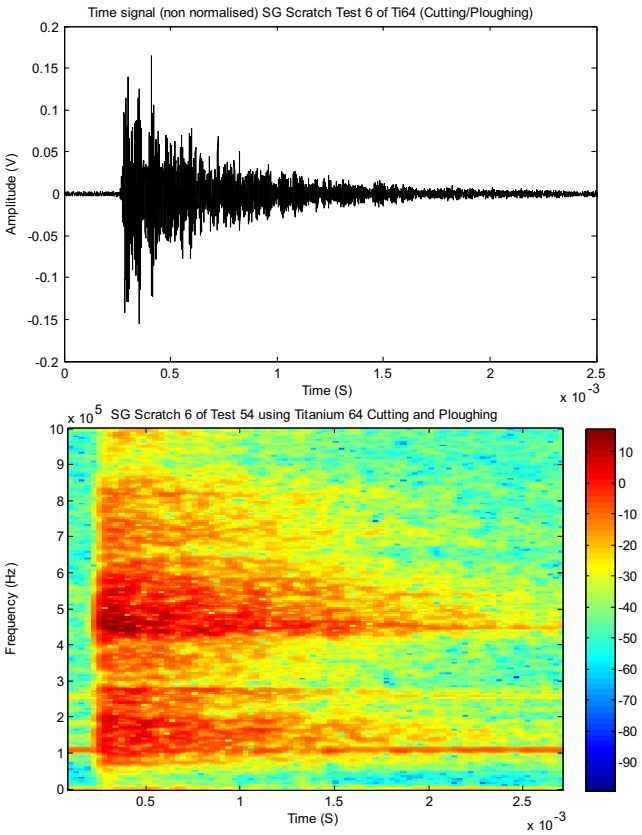

Fig. 11 *Top*, AE STFT of cutting/ploughing phenomenon for titanium 64 material (non-normalised). *Bottom*, STFT of TOP

Lastly, it was noticed from recorded AE signal phenomena that if a single piece of grit is used to make the scratch compared with a piece of grit with multiple edges, then there is more cutting phenomena found with the single piece of grit. This is indicative of a sharp non-worn piece of grit compared with a blunt fractured worn piece of grit. With further grit to material interaction the multiple piece of grit will breakdown to a single piece of grit significant of the self-sharpening grinding phenomenon.

5 Clustering method for classification of cutting, ploughing and rubbing in grinding

The primary pattern recognition technique used for classification is fuzzy-c clustering [9, 18, 24]. Pattern recognition can select features of interest when faced with many different features. The technique of fuzzy clustering provides rules in the form of distance measurements that segregate the different cluster sets from each other, in this case, the cutting, ploughing and rubbing.

Clustering techniques have emerged from work carried out in statistical probability [25, 26]. When looking at real world phenomena most cases are not finite and instead possess a lot of in-between values such as that seen in fuzzy sets. Essentially, clustering techniques use a distance measure to segregate like data from other presented data into classes or sets (clusters).

Figure 13 displays a block diagram of the fuzzy clustering/GA, which is based on work carried out by Griffin and Chen [18] clustering: cutting, ploughing and rubbing phenomenon's during SG tests. The first step in this process is to convert the STFT vectors into a fuzzy similarity matrix defining relations of similarity. The next process is to then define the fuzzy variable similarity matrix which evaluates each coefficients $\widetilde{r}_{ij}$ degree of membership between elements i and j. The cluster centres are then determined, where the centres segregate and categorise one cluster from another.

The centre cluster is the representing function of a particular cluster set. Input test data that has a membership close to a particular centre compared with other centres signifies that the applied input data belongs to that centre.

Let $X=\{X_1,X_2,\ldots,X_m\}, X\subset V$, where X_1 to X_m are feature vectors which make up the total feature matrix set and $X_i=(X_{i1},X_{i2},\ldots,X_{in})\in V$ is a feature vector (element of total feature matrix set V); X_{ij} is the jth feature of individual X_i; the feature matrix is made up from 1 to n feature vectors. To ensure there is normalisation across the feature matrix, Eq. (2) is applied which calculates the normalised mean for each input value divided by the variance.

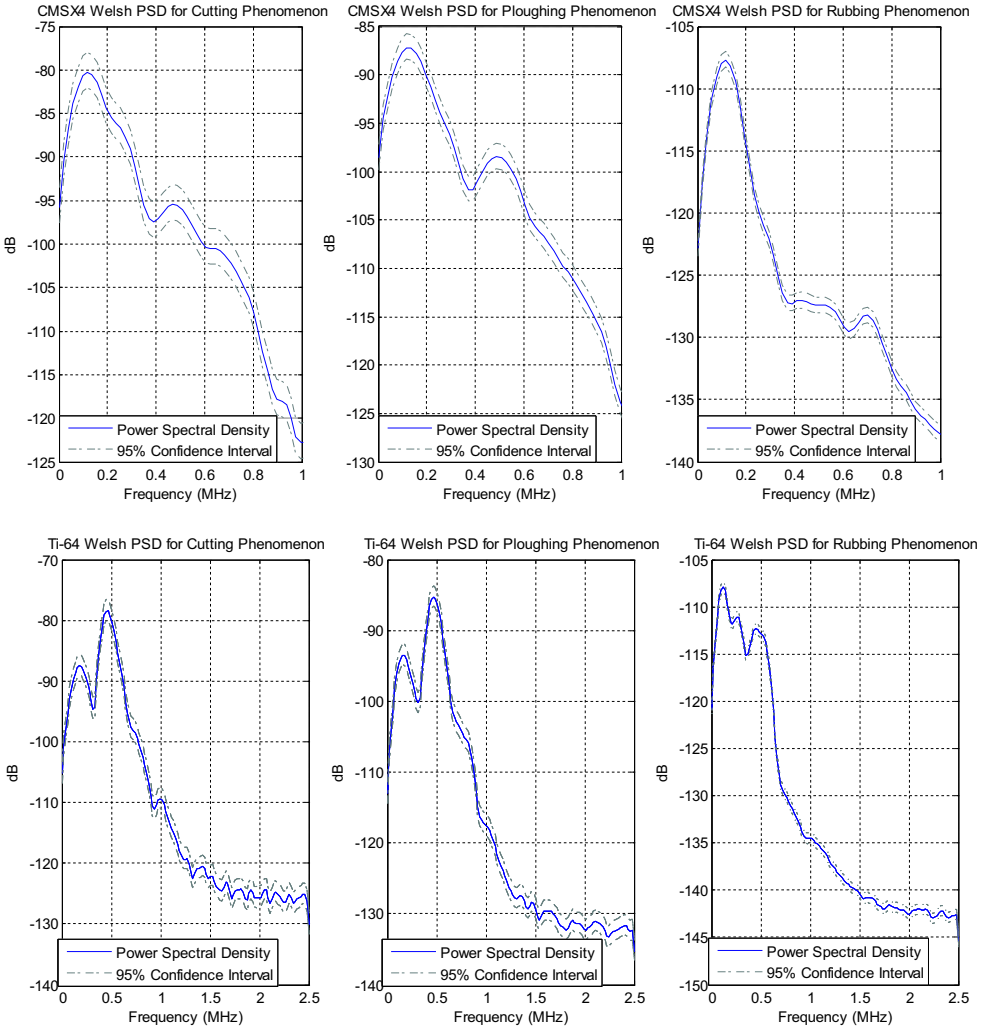

Fig. 12 *Top*, SG4 test 210 and 212 displaying the PSD of cutting, ploughing and rubbing using material CMSX4. *Bottom*, SG5 test 52 and 54 displaying the PSD of cutting, ploughing and rubbing using material titanium 64

$$x'_{ij} = m_j \times X_{ij} \text{ and } x''_{ij} = \left(x'_{ij} - \overline{x}'_i\right)/\sigma_i \tag{2}$$

Where:

$m_j = \max(X_{11}, X_{12}, \ldots, X_{1n})/X_{1j}$, $\quad \overline{x}_i{}' = \frac{1}{n}\sum_{j=1}^{n} x'_{ij}$ and

$$\sigma_i = \left|\frac{1}{n}\sum_{j=1}^{n}\left(x'_{ij} - \overline{x}_i{}'\right)^2\right|^{1/2}$$

The normalised feature matrix is then represented by the feature matrix below in Eq. (3).

$$X(m \times n) = \begin{bmatrix} x''_{11}, & x''_{12}, \ldots, x''_{1j}, \ldots, x''_{1n} \\ x''_{21}, & x''_{12}, \ldots, x''_{2j}, \ldots, x''_{2n} \\ \vdots & \vdots \\ x''_{il}, & x''_{i2}, \ldots, x''_{ij}, \ldots, x''_{in} \\ \vdots & \vdots \\ x''_{m1}, & x''_{m2}, \ldots, x''_{mj}, \ldots, x''_{mn} \end{bmatrix} \tag{3}$$

The fuzzy similarity matrix is the next calculation required for the fuzzy clustering of the input data set. The similarity matrix uses a distance measure to show similarities within the matrix set. There are many distance functions available; however fuzzy clustering uses Eq. (4). The index of similarity is based on the minimum distance that equates to the maximum similarity.

$$m_{ij} = \frac{\sum_{k=1}^{n}\left|\left(x_{ik} - \overline{x}_i\right)\left(x_{kj} - \overline{x}_j\right)\right|}{\left\{\left[\sum_{k=1}^{n}\left(x_{ik} - \overline{x}\right)^2\right] \times \left[\sum_{k=1}^{n} x_{kj} - \overline{x}_j\right)^2\right]\right\}^{\frac{1}{2}}} \tag{4}$$

By using the correlation coefficient Eq. (4), the normalised feature matrix is converted into a fuzzy proximity matrix M:

$$M = \begin{bmatrix} m_{11}, & m_{12}, & \ldots, m_{1j}, \ldots, m_{1n} \\ m_{21}, & m_{22}, & \ldots, m_{2j}, \ldots, m_{2n} \\ \vdots & & \vdots \\ m_{i1}, & m_{i2}, & \ldots, m_{ij}, \ldots, m_{in} \\ \vdots & & \vdots \\ m_{m1}, & m_{m2}, & \ldots, m_{mj}, \ldots, m_{mn} \end{bmatrix} \tag{5}$$

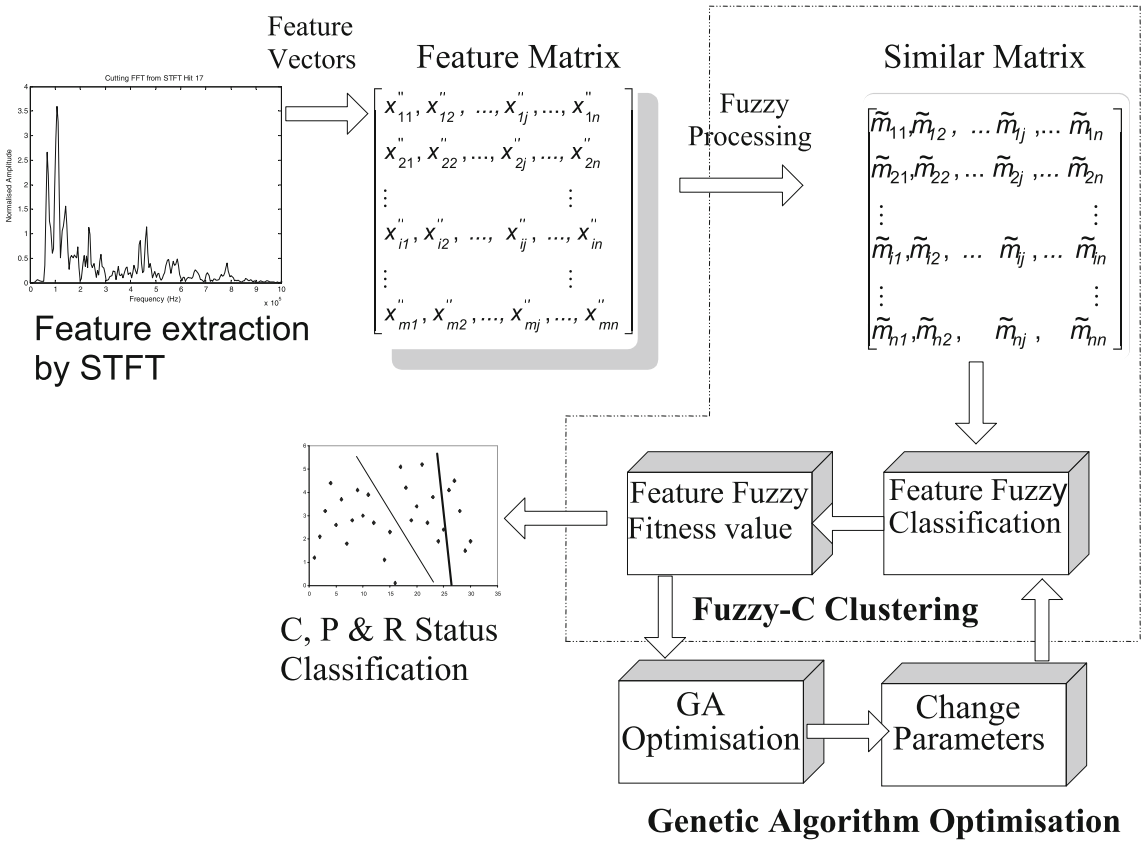

Fig. 13 Block diagram of the C, P and R classifications

The fuzzy proximity matrix M is then converted into a fuzzy similarity matrix M^K as the proximity relationship does not have enough similarities for fuzzy clustering to be carried out. From using the fuzzy algorithm such as transitive closure, the fuzzy matrix M can be converted into the fuzzy similarity matrix M^K.

$$M^K = \begin{bmatrix} \tilde{m}_{11}, \tilde{m}_{12}, \ldots, \tilde{m}_{1j}, \ldots, \tilde{m}_{1n} \\ \tilde{m}_{21}, \tilde{m}_{22}, \ldots, \tilde{m}_{2j}, \ldots, \tilde{m}_{2n} \\ \vdots \qquad\qquad \vdots \\ \tilde{m}_{i1}, \tilde{m}_{i2}, \ldots, \tilde{m}_{ij}, \ldots, \tilde{m}_{in} \\ \vdots \qquad\qquad \vdots \\ \tilde{m}_{m1}, \tilde{m}_{m2}, \ldots, \tilde{m}_{mj}, \ldots, \tilde{m}_{mn} \end{bmatrix} \tag{6}$$

$$\min\left\{ J_m = \sum_{j=1}^{m} \sum_{i=1}^{n} \left|\mu_j(x_i)\right|^b \left\|x_i - c_j\right\|^2 \right\} \tag{7}$$

Looking at Eq. (6), $\tilde{m}_{ij}$ in the matrix M^k is the similarity between features i and j. The maximum value of similarity is when $i=j$ and the feature itself equates to 1. After ranking the features in order of similarity values, it is then possible to segregate such features using the closest cluster distance membership function and distinguish the AE STFT data in terms of cutting, ploughing and rubbing phenomena. The closest distance membership function of fuzzy clustering is

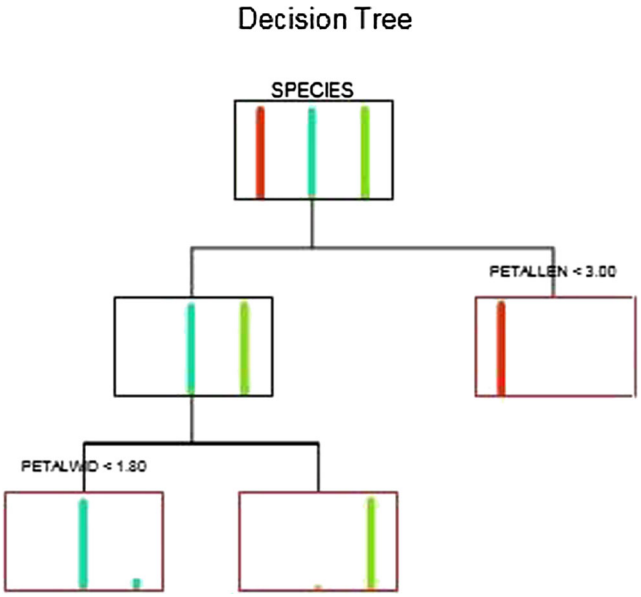

Fig. 14 CART example of classification rules [28]

Table 2 CART left and right branch values for different grit gains

Gain	L/right1	L/right 2	L/right3	L/right4	L/right5	L/right6	L/right7	L/right8
0.4	0.030926	0.393144	0.199154	0.0019177	0.548911	0.0016878	0.003711	
0.6	0.046389	0.589716	0.298732	0.0028766	0.823367	0.0025317	0.005566	0.009278
0.8	0.061852	0.786288	0.398309	0.0038355	1.09782	0.0033756	0.007422	
1.0	0.077315	0.98286	0.497886	0.0047944	1.37228	0.0042195	0.009278	

based on the squared loss-cost function (see Eq. 7) for each point. For Eq. 7, x_i is the samples (i=1, 2, …, n), m is the number of known clusters, c_j is the cluster centre point where (j=1, 2, …, m), $\mu_j(x_i)$ is the fuzzy membership of sample x_i to cluster j. If the b term equals to 1, it tends to lean more towards k-means clustering, similar to city-block distance statistical measure, and if b tends towards ∞, it becomes completely fuzzy, which is similar to Chebyshev maximum distance clustering. If, however, the term b takes the value of 2, it is similar to the Euclidean distance technique, which was used in this work. The fuzzy algorithm iterates through Eq. 7 until it can no longer best fit the separation of one cluster from another. This method was optimised by a GA where the cluster centres and number of iterations was optimised through the associated fuzzy-c clustering fitness coverage metric. Such ideas for optimised fuzzy clustering were inspired by previously presented work presented by Griffin and Chen [18].

6 Treeviewer rule-based method for classification of cutting, ploughing and rubbing in grinding verifying fuzzy clustering with GA optimisation

The treeviewer classifier uses the CART algorithm to carry out classification; CART is particularly useful in segregating n-dimensional data sets and produces transparent, easily readable set of classification rules. There are other techniques which are similar to optimised fuzzy clustering such as genetic programming (GP) as seen in a work discussed by Griffin and Chen [24]; however, when faced with n-dimensional data with no pre-processing reduction, other techniques are more favourable. Moreover, GP with n-dimensional reduction techniques affords a very powerful classification system; however, with n-dimensions, a different technique needs to be pursued. CART however is a method of classification similar to fuzzy clustering with the added facet of producing more transparent rules, which is why it has been used here to verify the output classifications of fuzzy clustering and easily transportable to real-time simulation. As mentioned before, CART is also suitable for n-dimensional datasets, which is what is presented here and by using pre-processing techniques in real time are unsuitable based on the increase in computational complexity which impacts on real-time processing.

CART builds classification and regression trees for predicting continuous dependent variables (regression) and categorical predictor variables (classification) [27]. It achieves its functionality by recursively splitting the feature space into sets of non-overlapping regions (rectangles in the case of continuous features; subsets of values, in the case of categorical features), and finally by predicting the most likely value of the dependent variable within each region. By generating a binary tree through recursive partitioning, it splits the data into sub-nodes based on the minimisation of a heterogeneity criterion computed at the resulting sub-nodes. With the CART algorithm, the tree is forwardly propagated (using forward stepwise regression) for best purity of node split. The best node split becomes the chosen value of partition (see Eq. 8).

A good splitting criteria is the following:

$$\begin{aligned} &\mathrm{PRE} = \emptyset(s,t) \\ &\text{Misclassification error}: Q_m = \frac{1}{N_m} \sum_{x_i \varepsilon R^m} (yi \neq k(m)) = 1 - \hat{P}_{mk(m)} \end{aligned} \quad (8)$$

Table 3 CART rule output for different grit gains

Gain	O/P cutting level	O/P ploughing level	O/P rubbing level
0.4	1.4	2.4	3.4
0.6	1.3	2.3	3.3
0.8	1.2	2.2	3.2
1.0	1	2	3

```
Decision tree for classification for SG gain of 0.4:
 1  if x73<left1 then node 2 elseif x73>=right1 then node 3 else 3.4
 2  if x23<left2 then node 4 elseif x23>=right2 then node 5 else 3.4
 3  if x38<left3 then node 6 elseif x38>=right3 then node 7 else 2.4
 4  if x118<left4 then node 8 elseif x118>=right4 then node 9 else 3.4
 5  class = O/P Ploughing Level
 6  if x34<left5 then node 10 elseif x34>=right51 then node 11 else 2.4
 7  if x3<left6 then node 12 elseif x3>=right6 then node 13 else 1.4
 8  class = O/P Ploughing Level
 9  class = O/P Rubbing Level
10  if x174<left7 then node 14 elseif x174>=right7 then node 15 else 2.4
11  class = O/P Cutting Level
12  class = O/P Ploughing Level
13  class = O/P Cutting Level
14  class = O/P Rubbing Level
15  class = O/P Ploughing Level
```

Fig. 15 CART rules for gains 0.4 to 1 of the C, P and R classifications

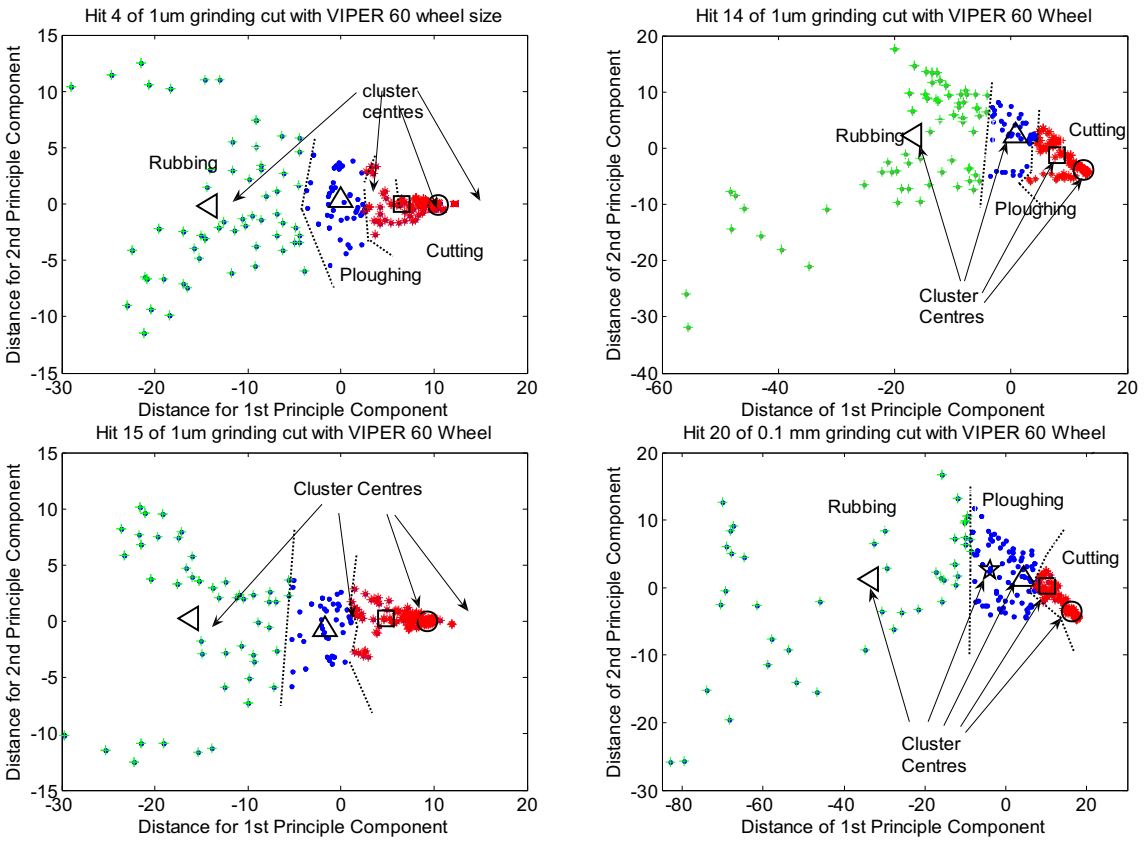

Fig. 16 Fuzzy-c clustering: *top left*, hit 4; *top right*, hit 14; *bottom left*, hit 15 of 0.1 μm cut; and *bottom right*, hit 20 of 0.1 mm cut

Where y_i is the output of the individual under test and k (m) is the class category under test. PRE is the minimum production reduction in error, s is the spilt at any t node. The best purity measure looks at the best unique class classification where less impure looks at more multiclass representation. For the CART algorithm, the percentage accuracy of classifications is used as the best purity measure.

This method of classification is not only chosen to verify fuzzy clustering and rule transparency but also because the tree fitting methods are actually closely related to cluster analysis [26]. This is where each node can be thought of as a cluster of objects, or cases, which are split by further branches in the tree. Note that the top node covers the whole sample amount and each remaining node contains a subamount of the original sample and so on as the split levels increase.

In the example shown in Fig. 14, the total data set can be seen from species at the top node of the tree classifier. The condition of Petal len is the first variable and if species is less than 3.00, then the data class category will tend towards the right-hand side split (example, displaying

Table 4 Fuzzy clustering results for 1 μm cuts and 0.1 mm cut

Test set	Fuzzy GA cutting (C)	Fuzzy GA ploughing (P)	Fuzzy GA rubbing (R)	Classification accuracy %
Test SG4	61/62	43/47	81/97	90 % (185/206)
Hit 3 T211 (rubbing)	53/55	51/66	84/85	91 % (188/206)
Hit 2 T212	52/55	60/66	84/85	95 % (196/206)
Hit 4* (*1 μm cut)	69/69	41/50	71/87	88 % (181/206)
Hit14*	42/48	58/59	68/99	82 % (167/206)
Hit15*	46/46	72/96	55/64	84 % (173/206)
Hit 20 (0.1 mm cut)	39/44	82/85	77/77	96 % (198/206)

Table 5 The fuzzy cluster clustering for the percentage of C, P and R phenomenon

Test set	C%	P%	R%	Iterations and clusters	Fitness
Test SG4	33 % (20/60)	23 % (19/60)	44 % (21/60)	78/4	0.7245
Hit 3 T211 (rubbing)	0 % (0/21)	0 % (0/21)	100 % (21/21)	190/6	0.822
Hit 2 T212	32 % (12/38)	61 % (23/38)	8 % (3/38)	153/5	0.1305
Hit 4 (1 μm cut)	19 % (9/47)	26 % (12/47)	55 % (26/47)	135/6	1.659
Hit 14 (1 μm cut)	52 % (30/58)	23 % (13/58)	21 % (12/58)	81/4	0.8862
Hit 15 (1 μm cut)	58 % (36/62)	24 % (15/62)	18 % (11/62)	165/6	1.85
Hit 20 (0.1 mm cut)	76 % (48/60)	22 % (13/60)	2 % (1/60)	120/5	0.968

the red line class). If, however, the Petal len is greater or equal to 3.00, then the left-hand branch is taken, splitting the remaining part of the total data set. Lastly, the last branch has a second condition for a second parameter providing both further splits right and left. If Petal wid is less than 1.30 then the left-hand branch is taken otherwise, the right-hand branch. This is a simple example of flower stork length classification but displays the functionality behind the CART classification algorithm.

A classification tree represents a set of nested logical if–then conditions (similar to a rule-based system) on the values of the feature variables that allows the prediction of the value for the dependent categorical variable based on the observed values of the feature variables. A regression tree also represents a set of nested logical if–then conditions on the feature variables, but these are used instead to predict the value of a continuous response variable.

CART can handle missing values by imputing such values in obtaining the mean over the complete observations. The model can be tested on a separately specified test set. Additionally, the model can be saved and used subsequently on additional test sets.

Some points for discussion on best tree representations are as follows:

- A very large tree may overfit the data.
- A small tree might not capture the important structure

Therefore, there is trade-off consideration for the best tree when thinking of the overall size:

- The optimal tree size should be adaptively chosen from the data provided.
- Different stopping criteria's can give different results such as an impurity threshold is reached and the branching and splitting is halted or a specified minimum of branch level is achieved and so branching and splitting is halted at this point.
- Think of a pruning strategy that does not impact on the overall tree classification accuracy.

6.1 Limitations of trees

One important consideration is based on the high variance of output based on its hierarchical nature to classify. A small change in data may result in different splits, thus making such interpretations precautious. Errors are made from the top node filter down to the lower nodes. All tests carried out using this technique were verified against test and verification unseen data sets. With high classifications, confidence in this method is achieved.

Tables 2 and 3, used in conjunction with Fig. 15, display the input and output values for the different gain CART rules.

With a test set classification of 54/60 which signifies a 90 % classification accuracy verifies CART against the fuzzy clustering technique, and with both classifiers, it is possible to give a robust overall controller. Such classification predictions were formed for all different gain level rules (see Fig. 15; Tables 2 and 3). The 23rd parameter (X23) was used to trigger which specific gain rule would be fired based on a detected level.

7 Classification of cutting, ploughing and rubbing

The section presents the classifications for fuzzy clustering and CART classifications.

7.1 Fuzzy clustering classifications

Figure 16 displays the first two principle component outputs based on the two principle components with the highest evaluated data cluster centre membership.

It would appear that the fuzzy-clustering/GA technique has given similar results to previous work [18], and therefore the findings in this paper are conclusive of the cutting, ploughing and rubbing phenomena distinguished by the energy released from the workpiece and grit interaction in the form of an AE signal.

Table 4 displays the known classification accuracy of fuzzy clustering. Here, the correct/incorrect clusters were checked against the known phenomenon, and a percentage of

Table 6 CART results for 1 μm cuts and 0.1 mm cut

Test Set	FuzzyGA cutting (C)	FuzzyGA ploughing (P)	FuzzyGA rubbing (R)	Classification accuracy (%)
Test SG4	61/62	45/47	95/97	98 % (201/206)
Hit 3 T211 (rubbing)	54/55	63/66	84/85	98 % (201/206)
Hit 2 T212	52/55	61/66	81/85	94 % (194/206)
Hit 4* (*1 μm cut)	66/69	46/50	81/87	96 % (193/206)
Hit 14*	45/48	58/59	91/99	94 % (194/206)
Hit 15*	43/46	92/96	61/64	96.5 % (196/206)
Hit 20 (0.1 mm cut)	39/44	80/85	77/77	96.5 % (196/206)

classification was determined. Table 5 displays the percentage of cutting, ploughing and rubbing phenomenon for hits 4, 14 and 15 (0.1 μm DOCs) and hit 20 (0.1 mm DOC).

From looking at Table 5, it is possible to see more utilisation of cutting, then ploughing and rubbing when the DOC increases towards the centre of the workpiece leading to more interaction between grit and workpiece.

7.2 CART classifications

Table 6 displays the known classification accuracy of CART classifications. Table 7 displays the percentage of cutting, ploughing and rubbing phenomenon for hits 4, 14 and 15 (0.1 μm DOCs) and hit 20 (0.1 mm DOC).

Again from looking at Table 7, it is possible to see more utilisation of cutting, then ploughing and rubbing when the DOC increases towards the centre of the workpiece leading to more interaction between grit and workpiece. This is consistent with the results tabulated in Table 5. Both classifications have dis/advantages to classifying data, and when used as a dual-classification system, more robustability is achieved (Fig. 24).

8 Single-grit simulation

Simulations are very important for both real-time controllers and high fidelity models. Figure 17 displays a flow chart for the internal workings of the SG simulation.

From the identification and classification of the AE signal analysis against measured material phenomenon, it is possible to realise such findings in a simulation for real-time application/modelling. Such micro-grinding simulation models can act as more informed mechanics when scaled up to the macro-grinding models as opposed to using a random distribution of possible grit interaction seen in work [29].

Figures 18, 19 and 20 display all the main sub-systems that make up the functionality of real-time simulation. Figure 18 displays the top-level view of the simulation, with the neuro-fuzzy clustering SOM coloured in blue. The green parts are various CART rule-based systems depending on the identified level of X23 (23rd element of data from STFT). The rest displays from the left, the random firing of signals (time to STFT). After both blue and green classifier parts, there is the combiner for robust classifier output (Fig. 18, middle). Figures 19 and 20 display the neuro-fuzzy clustering SOM into three layers, where Fig. 19 is the top layer of the SOM network, and Fig. 20 the input layer significant of 256 inputs representative of the STFT input signal(s) (hidden and output layers follow a similar pattern).

The simulation displayed in Fig. 18 shows different time-frequency FFT samples tested against a neuro-fuzzy clustering SOM (closest method to fuzzy clustering with GA optimisation). Using a decreased gain classifier input signifying material phenomenon's tending towards a ploughing or rubbing grit action, the classifier gives output for necessary sharpening phenomena such as dressing to take place. Figure 21 displays the SOM simulation output for different gains, signifying different levels of grit action with increasing tendency towards blunting phenomenon (when red = 1). The blue output gives the classification of signals inputs in terms of cutting, ploughing and rubbing.

Figure 22 gives the SOM classifier output in terms of percentage utilisation of the phenomena: cutting, ploughing

Table 7 The CART classification for the percentage of C, P and R phenomenon

Test set	C%	P%	R%
Test SG4	31.6 % (19/60)	35 % (21/60)	33.3 % (20/60)
Hit 3 T211 (rubbing)	0 % (0/21)	0 % (0/21)	100 % (21/21)
Hit 2 T212	6 % (2/38)	76 % (29/38)	18 % (7/38)
Hit 4 (1 μm cut)	8 % (4/47)	49 % (23/47)	43 % (20/47)
Hit 14 (1 μm cut)	52 % (30/58)	19 % (11/58)	29 % (17/58)
Hit 15 (1 μm cut)	63 % (39/62)	29 % (18/62)	8 % (5/62)
Hit 20 (0.1 mm cut)	92 % (55/60)	8 % (5/60)	0 % (0/60)

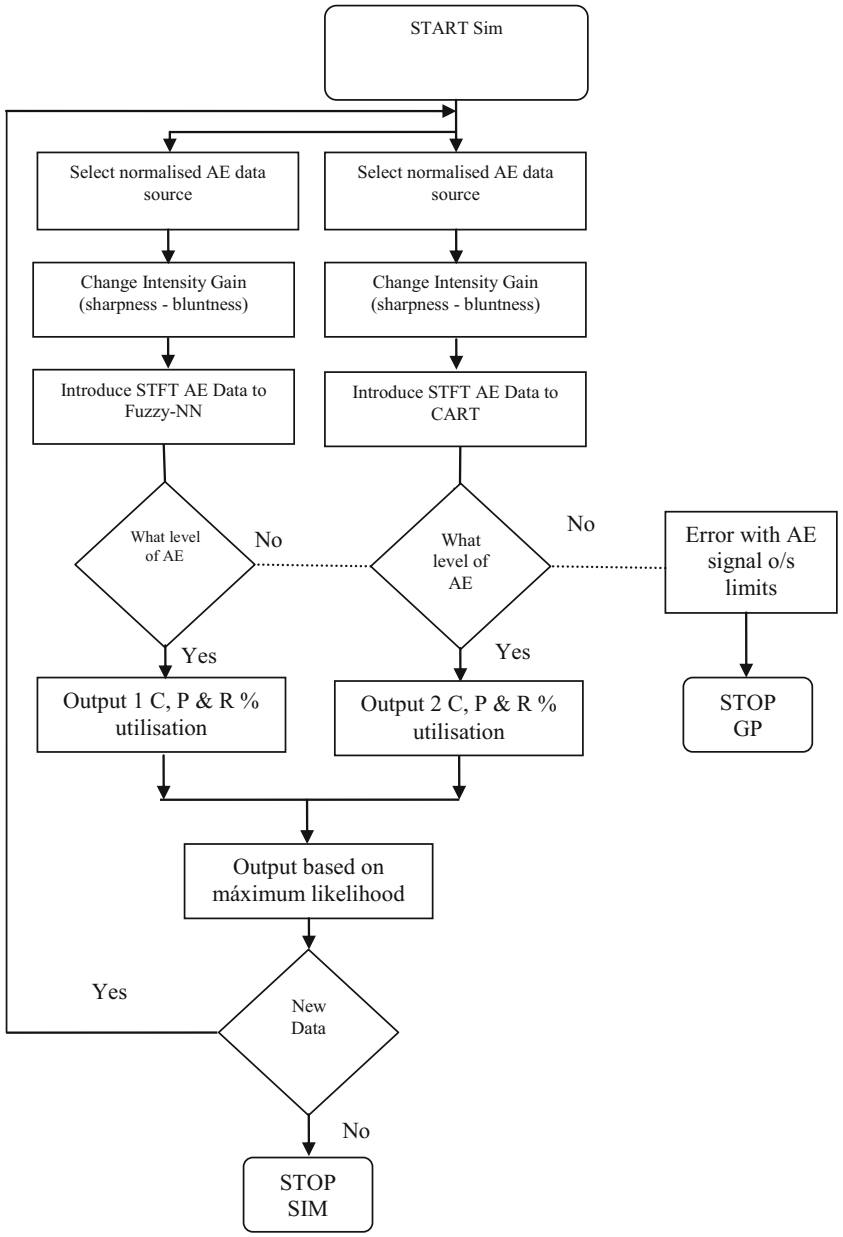

Fig. 17 Flow chart of fuzzy SG expert system

and rubbing. This crisp percentage output (0–1, 0–100 %) is given by the neuro-fuzzy clustering SOM, which is typical of such technologies in the ability to output merged cluster sets. This output is more accurate than that displayed in Fig. 24 (due to the CART rules translation from individual CART to embedded simulation rules where the firing rules mechanism can be different); however, with both the sharpening control and percentage phenomenon utilisation, this promotes a more informed dressing control process. CART was verified with a higher accuracy than that of neuro-fuzzy clustering SOM (see Tables 4 and 5 compared with Tables 6 and 7) and is not displayed here in terms of percentage utilisation as this is the negative from both Figs. 23 and 24 compared 8with Figs. 21 and 22, respectively. CART is used as a secondary classifier to verify neuro-fuzzy clustering SOM.

Certainly, CART is more transparent and better adopted for dealing with *n*-D data than neuro-fuzzy clustering SOM; and, it can deal with *n*-D data and has the ability to regress outputs giving good predictions. Combined with CART rules, the sensitivity of the neuro-fuzzy system is slightly desensitised giving more robust classifications. Even though the CART algorithm gave a +90 % classification of unseen data, there was less weighting applied in the fuzzy combination due the neuro-fuzzy clustering SOM, giving better regression capabilities where such weightings were based on 30 % of the CART output and 70 % of neuro-fuzzy

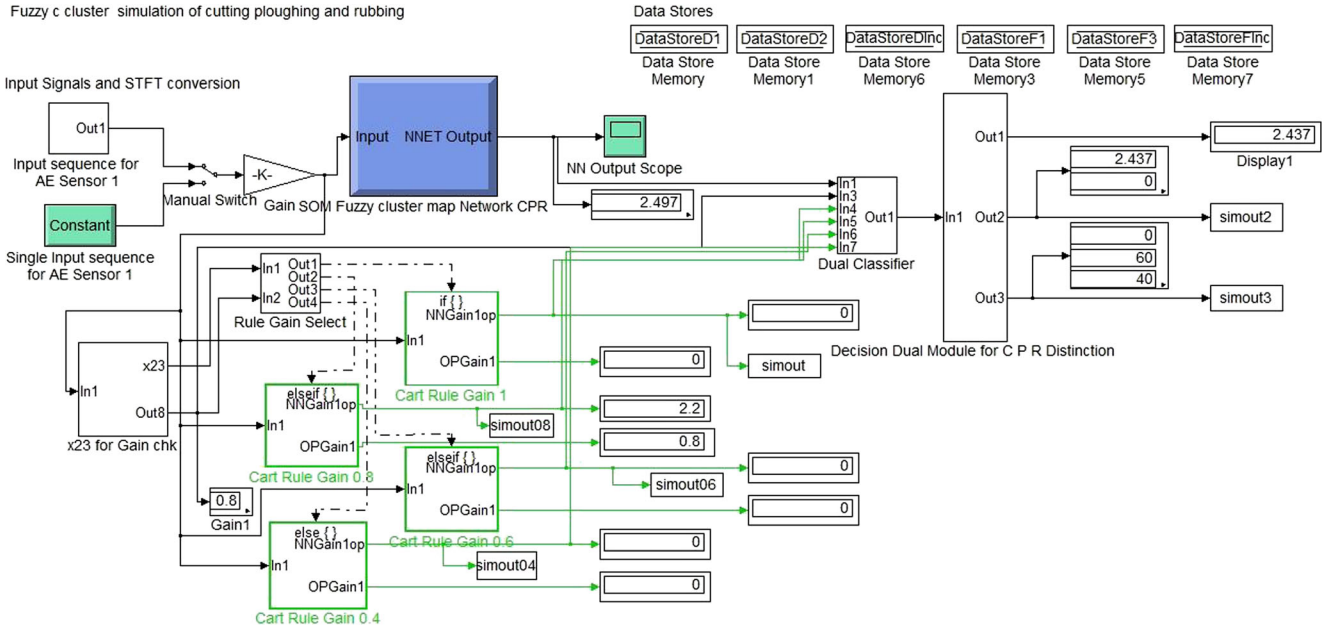

Fig. 18 Top-level simulation for SG phenomena classifications

clustering SOM output. This type of classifier can be considered as both accurate and robust and can be used for either modelling or control purposes. One point to note here is different rules have to be found with the CART when faced with different data (gain changed data), whereas the neuro-fuzzy system can regress from the original data when faced with different gain changed data. That said, for CART to act the same, the variables used in the node can be replaced for probabilities and adjusted for various gain changes, in short: a hybrid feedback CART system.

Figures 23 and 24 display the output control and output percentage utilisation, respectively, for the neuro-fuzzy and CART rules system. Here, it can be seen that the output spikes at a lower rate than in Figs. 21 and 22, which is based on the dual combination of CART and neuro-fuzzy classifications. The dual classification system certainly gives a smoother output albeit similar to the neuro-fuzzy system output based on the bias of the combiner fuzzy weightings.

That said, Fig. 24 (bottom right for 0.4 gain) displays a more accurate classification towards the end, which is given by the dual classifier. The individual CART rules for the simulation were based on Fig. 15 and Tables 2 and 3 (0.4 to unit gain).

9 Conclusions

This paper has demonstrated that STFT as a useful technique to distinguish the frequency bands occupied by cutting, ploughing and rubbing phenomena with high classification accuracy (+90 %) for both classifying technologies. Two different aerospace materials CMSX4 and Titanium 64 were compared in terms of STFT signal characteristics showing similar consistencies with respect to DOC and intensity amounts; however, with materials with higher hardness and density values, there is more material damping when subject

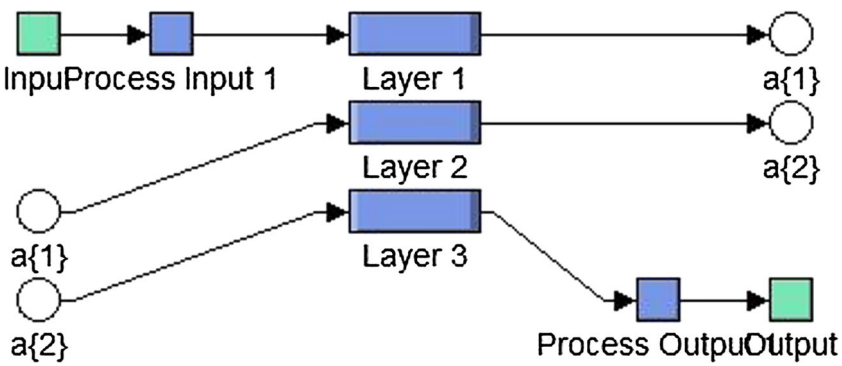

Fig. 19 Top level of neuro-fuzzy clustering SOM for SG phenomena classifications

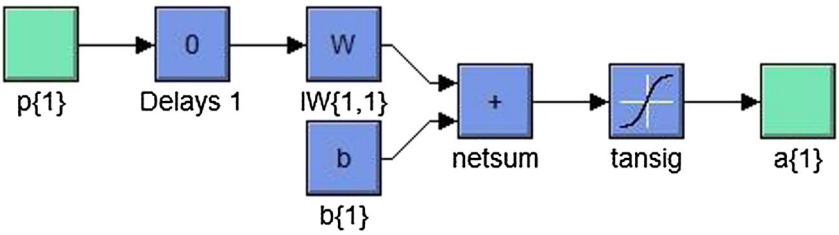

Fig. 20 Layer 1 (input layer) of neuro-fuzzy clustering SOM

to an emitted AE event. Two different aerospace materials CMSX4 and Titanium 64 were compared in terms of STFT signal characteristics showing similar consistencies in DOC and intensities.

Cutting and ploughing were difficult to distinguish due to their similar plastic material energy properties. However, from material measurements, the amount of material removed against material built up edge would clarify either cutting or ploughing phenomenon. Rubbing was difficult to distinguish from noise as the noise levels are in-between identified rubbing phenomenon. Rubbing is verified from the obtained AE hit data signal correlated to no visible mark on the workpiece or more AE signal data compared with actual scratch length. The rubbing phenomenon is different from both cutting and ploughing phenomena, where it contains only elastic deformation energy properties and ploughing/cutting has plastic deformation energy properties. With elastic deformation, there should be no or very little marking on the workpiece surface. The non-normalised signal analysis was consistent with other SG work [23]; however, for a generalised classifier of cutting, ploughing and rubbing, such signals were normalised to 1 μm DOC. The DOC is an important feature in SG grinding where a separate classifier can be used to convey such information within a SG grinding model. The fuzzy clustering method gave high classification results and was verified by a similar fuzzy-type rule-based system: CART. The transparent CART achieved higher accuracies than the optimised fuzzy clustering; however, different rules are needed to extrapolate the data accommodating different grit gains where fuzzy clustering implemented through a SOM NN has such abilities built into its functionality and is therefore more versatile to change. Both technologies have their advantages and disadvantages, and when used in a

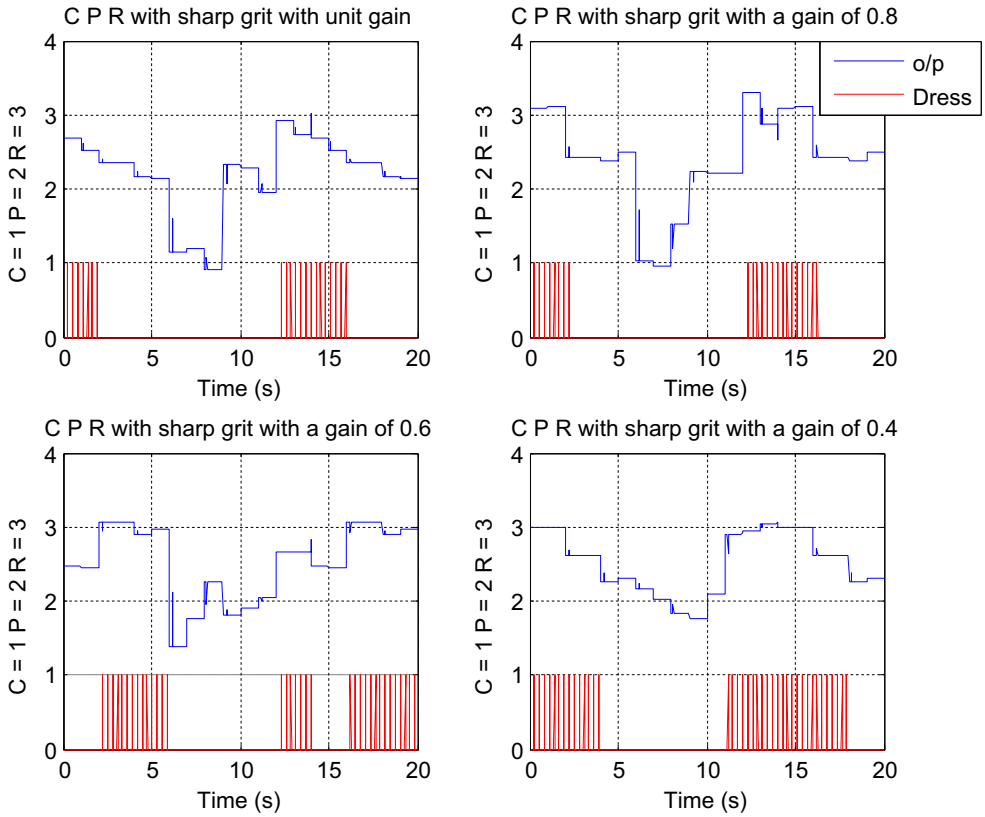

Fig. 21 Simulation for SG phenomena classifications with changing gain signifying a blunting of grit after constant material interaction using neuro-fuzzy clustering SOM

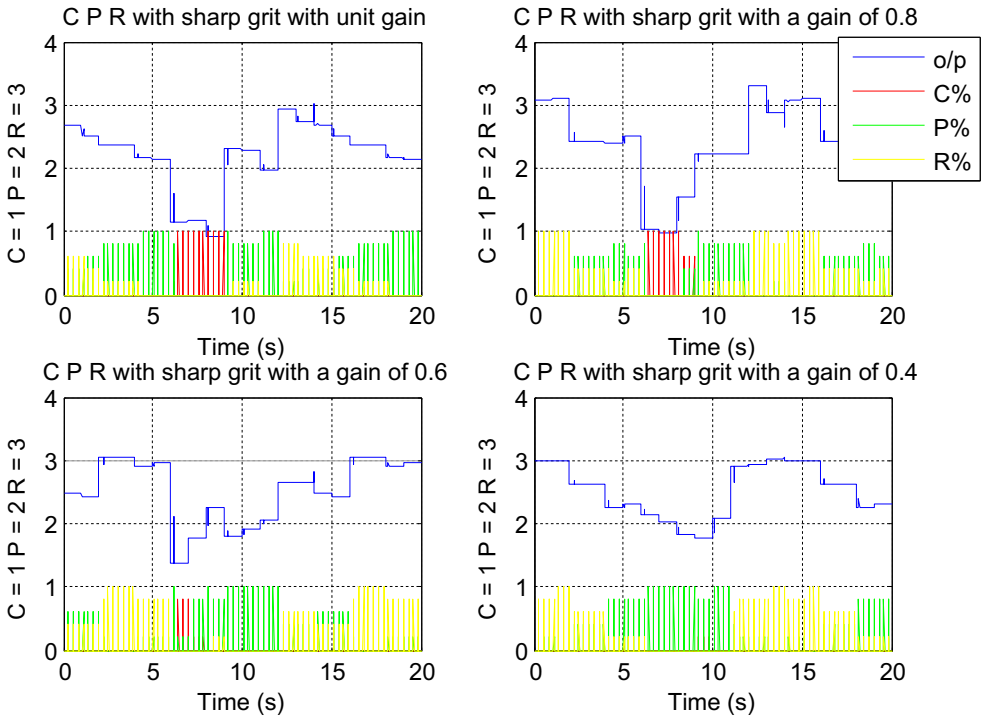

Fig. 22 Simulation for SG phenomena classifications with changing gain signifying a percentage output of the phenomenon's: cutting, ploughing and rubbing using neuro-fuzzy clustering SOM

hybrid fashion, affords a very powerful classification technique.

Further tests looked at AE hit data taken from macro-grinding with 1-μm and 0.1-mm depth cuts, where the classifier distinguished more percentage of cutting utilisation when the process had more interaction between workpiece and grit interaction (i.e. measured increased actual depth cut ending towards the middle of the workpiece).

Finally, such classifier results were realised in a simulation that could serve as a possible real-time controller for monitoring the levels of cutting, ploughing and rubbing for SG and small DOC grinding wheel material interactions. Considering

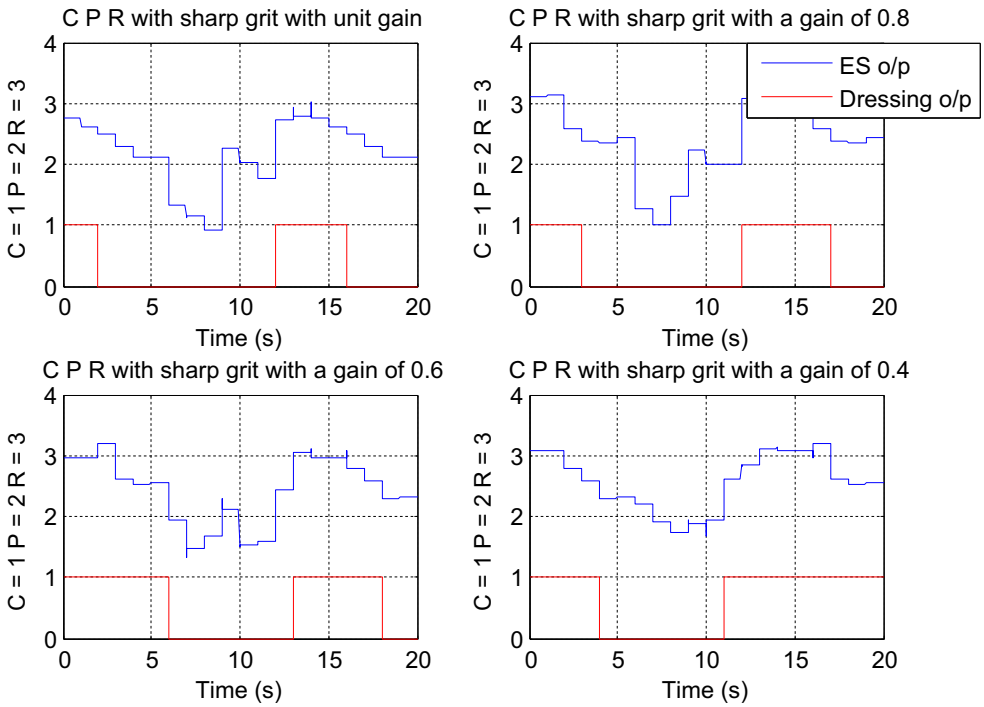

Fig. 23 Simulation for SG phenomena classifications with changing gain signifying a blunting of grit after constant material interaction using both neuro-fuzzy clustering SOM and CART rules for robust control

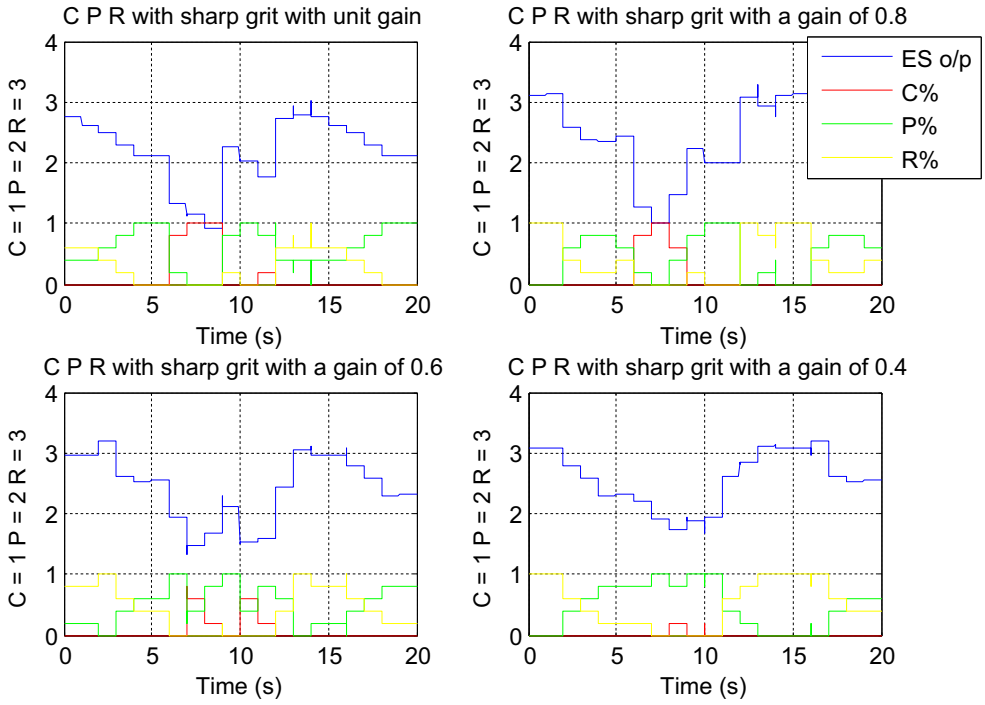

Fig. 24 Simulation for SG phenomena classifications with changing gain signifying a percentage output of the phenomenon's: cutting, ploughing and rubbing using both neuro-fuzzy clustering SOM and CART rules for robust control

the difficult segregation between cutting and ploughing, a percentage utilisation of the phenomena is also given as output from the simulation. Such percentage utilisation of grit to workpiece interactions are made possible by different cluster sets.

Investigation summaries: a more improved robust SG model is provided to give micro-mechanics of grinding from extracting AE signals, micro-grinding control regime, improved identification of cutting, ploughing and rubbing phenomena during grinding, promoting efficient grinding with more accurate grinding dressing ratios and, an intelligent material footprint-identification system.

References

1. Royer D, Dieulesaint E (2000) Elastic waves in solids I, II. Springer, Berlin
2. Smith SW (1997) The Scientist and Engineer's Guide to Digital Signal
3. Griffin J, Chen X (2009) Characteristics of the acoustic emission during horizontal single grit scratch tests—part 1 characteristics and identification. International Journal Abrasive Technologies—Special Issue on: "Micro/Meso Mechanical Manufacturing (M4 Process)". Vol., 1, No 4
4. Chen X, Griffin J, Liu Q (2007) Mechanical and thermal behaviours of grinding acoustic emission. Int J Manuf Technol Manag (IJMTM) 12(1~3):184–199
5. Webster J, Marinescu I, Bennett R (1994) Acoustic emission for process control and monitoring of surface integrity during grinding. Ann CIRP 43(1):299–304
6. Coman R, Marinescu ID et al (1999) Acoustic emission signal—an effective tool for monitoring the grinding process. Abrasives
7. Chen M, Xue BY (1999) Study on acoustic emission in the grinding process automation. American Society of Mechanical Engineers, Manufacturing Engineering Division, MED Manufacturing Science and Engineering—1999 (The ASME International Mechanical Engineering Congress and Exhibition), Nov 14–Nov 19 1999, Nashville, TN, USA, ASME, Fairfield, NJ, USA
8. Holford KM (2000) Acoustic emission—basic principles and future directions. Strain 36(2):51–54
9. Li X (1998) Tool wear monitoring with wavelet packet transform-fuzzy clustering method. Wear 219(2):145–154
10. Subhash G, Loukus JE, Pandit SM (2001) Application of data dependent systems approach for evaluation of fracture modes during single-grit scratching. Mech Mater 34:25–42
11. Wang H, Subhash G (2002) An approximate upper bound approach for single-grit rotating scratch with a conical tool on pure metal. Wear 252:911–933
12. Hamed MS (1977) Grinding mechanics—single grit approach. Ph,D. thesis, Leicester Polytechnic
13. Clausen R, Wang CY, Meding M (1996) Characteristics of acoustic emission during single diamond scratching of granite. Ind Diam Rev 3:96–99
14. Xiaoli L, Yingxue Y, Zhejun Y (1997) On-line tool condition monitoring system with wavelet fuzzy neural network. J Intell Manuf 8: 271–276
15. Ren Q, Balazinski M, Baron L (2012) Fuzzy identification of cutting acoustic emission with extended subtractive cluster analysis. Nonlinear Dynamics. 67(4), pp 2599–2608. *Processing* California Technical Publishing, ISBN 0-9660176-3-3
16. Ren Q, Balazinski M, Jemielniak K, Baron L, Achiche S (2013) Experimental and fuzzy modelling analysis on dynamic cutting force in micro milling. Soft Comput 17:1687–1697
17. Strang G, Nguyen T (1996) Wavelets and filter banks. Wesley Cambridge Press, ISBN 0-9614088-7-1, pp 1–29 61–68
18. Griffin J, Chen X (2009), Characteristics of the acoustic emission during horizontal single grit scratch tests—part 2 classification and

grinding tests. International Journal Abrasive Technologies—Special Issue on: "Micro/Meso Mechanical Manufacturing (M4 Process)". Vol., 1, No 4
19. Barbezat M, Brunner AJ, Flueler P, Huber C, Kornmann X (2004) Acoustic emission sensor properties of active fibre composite elements compared with commercial acoustic emission sensors. Sensors Actuators 114:13–20
20. Boczar T, Lorenc M (2006) Time-frequency analysis of the calibrating signals generated in the Hsu–Nielsen system. Phys Chem Solid State 7(3):585–588
21. Hwang TW, Whitenton EP, Hsu NN, Blessing GV, Evans CJ (2000) Acoustic emission monitoring of high speed grinding of silicon nitride. Ultrasonics 38:614–619
22. Kalpakjian S, Schmid SR (2003) Manufacturing process for engineering materials. Prentice Hall, ISBN 0-13-040871-9, pp 510–520
23. Opoz T, Chen X (2012) Experimental investigation of material removal mechanism in single grit grinding. Int J Mach Tools Manuf 63:32–40
24. Griffin J, Chen X (2009) Multiple classification of the acoustic emission signals extracted during burn and chatter anomalies using genetic programming. Int J Adv Manuf Technol 45(11–12):1152–1168
25. Cuevas A, Febrero M, Fraiman R (2001) Cluster analysis: a further approach based on density estimation. Comput Stat Data Anal 36: 441–459
26. Hartigan J (1985) Statistical theory in clustering. J Classif 2:63–76
27. Breiman L, Friedman J, Olshen R, Stone C (1984) Classification and regression trees. Wadsworth, Belmont
28. Coppersmith D, Hong SJ, Hosking JRM (1999) Partitioning nominal attributes in decision trees. Data Min Knowl Disc 3:197–217
29. Huang-Cheng C, Wang JJ (2008) A stochastic grinding force model considering random grit distribution. Int J Mach Tools Manuf 48(12–13):1335–1344